Images of gas molecules by electron holography. II. Experiment and comparison with theory

L. S. Bartell and W. J. Gignac

Department of Chemistry, The University of Michigan, Ann Arbor, Michigan 48109
(Received 26 October 1978)

Molecular images photographed by a variant of holographic microscopy proposed in Paper I are presented. "Holograms" were taken with an electron beam of 0.06 Å wavelength recorded up to a numerical aperture of 0.2 to yield an Abbe resolution limit of 0.15 Å. Experimental requirements and procedures are described. Images, representing rotational averages over an ensemble, closely resemble images calculated according to the theoretical expressions derived in Paper I. The theoretical treatment took into account the degradative effects of the zeroth-order beam transmitted through the hologram, finite numerical aperture and wavelength, the "false" peaks arising from the cutoff of the holograms at their centers, and nonoptimum first-stage filter functions. Illustrative examples include AsF_5, a case chosen to satisfy standard holographic requirements, and two cases, SF_5Cl and CF_3OOCF_3, selected to produce more complicated images.

I. INTRODUCTION

In Paper I,[1] a theoretical development was presented for a variant of electron-wave holography capable, in principle, of yielding rotationally averaged images of gas-phase molecules. If certain conditions are met, all terms arising in the new treatment are exactly analogous to those encountered by Gabor in his original treatment of holography.[2] Even when these conditions are not met, structural features of molecules can be reconstructed optically. It is the purpose of the present paper to learn what sorts of images can be obtained experimentally with current hardware, to calculate image amplitudes and image intensities corresponding to various experimental conditions, and to compare theoretical images with those found experimentally. Notation will follow that of Paper I.

II. EXPERIMENTAL PROCEDURE

A. Recording of electron-wave holograms

Holograms satisfying conventional holographic criteria can be made from ordinary Fraunhofer electron diffraction patterns of gas molecules containing one moderately heavy atom, provided a suitable filter (rotating sector) is used. For optimum results the filter function Φ should make the "atomic" intensity received at the recording emulsion, or

$$I_{at} = K_e \Phi \cos^3\theta_e \left\{ \sum_i \left[|f_i|^2 + (2/a_0 s_e^2)^2 S_i \right] \right\}, \qquad (1)$$

a constant function of scattering angle θ_e. While such filtering is possible, it would require a different rotating sector to be fashioned for each different type of molecule. For simplicity we investigated, theoretically and experimentally, whether acceptible images could be reconstructed with a much cruder compensation for the strong θ_e dependence of the scattering factors f_i. As a compromise we tried plates taken with a sector function Φ proportional to the cube of the sector radius—an ordinary "r^3" sector—and obtained reconstructions of sufficient quality that more complex sectors did not seem warranted in this initial study. In Fig. 1 is plotted the absorbance of a diffraction plate of AsF_5 filtered with an r^3 sector; its atomic background intensity deviates conspicuouly but not fatally from a constant.

Diffraction plates were taken with an electron diffraction apparatus described in detail elsewhere,[3,4] and recorded on 4 in.×5in. Process Plates or Electron Image Plates using a 40 kV beam of about 0.5 μA. The rotating sector had an excellent figure in the range of about $3 < s_e < 22$ at the 21 cm camera geometry used, and was blocked off at larger and smaller radii. Patterns of gaseous samples of AsF_5, SF_5Cl, and CF_3OOCF_3 were selected. Each had been taken in previous studies[5–7]; experimental conditions are given in Refs. 5–7.

Patterns recorded as described give surprisingly faithful blackenings as a function of intensity received. Absorbances, integrated around the pattern at constant impact parameter b_e (see Fig. 2 of Paper I) follow intensity modulations to a fraction of a part per thousand of the intensity. Nevertheless, the patterns are not suitable for holograms because of the exceptionally stringent requirements for spatial coherence in the reconstruction stage. The light beam of the optical synthesizer, after transmission through the full aperture

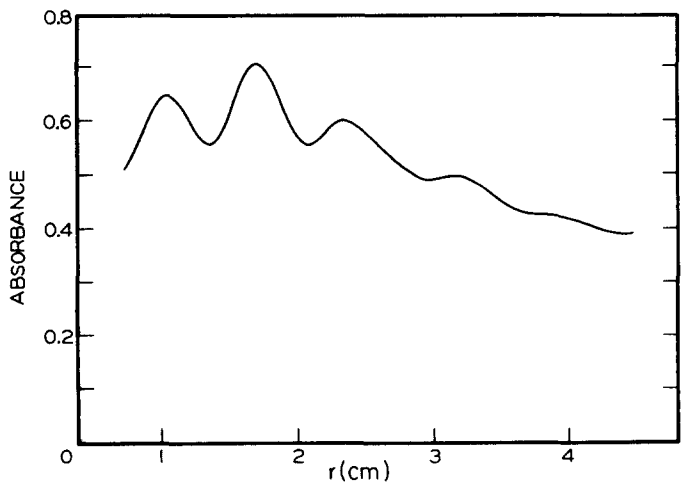

FIG. 1. Absorbance of electron diffraction pattern of AsF_5 transmitted through an r^3 sector filter; plotted as a function of plate radius.

 0021-9606/79/083958-07$01.00 © 1979 American Institute of Physics

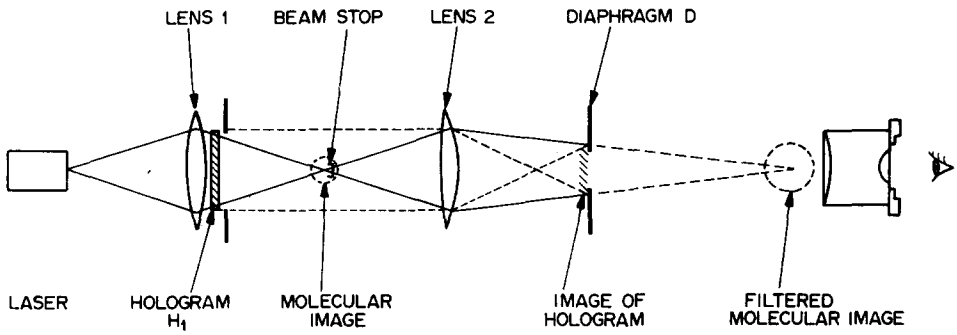

FIG. 2. Schematic diagram of optical reconstruction stage of holographic "microscope." The The optics from the beam stop to the ocular serve to filter out most of the unwanted amplitude propagating from $U_0(s)$ of Eq. (6).

of the hologram, must be able to be brought to a focus blurred only by the theoretically expected Airy diffraction pattern if the full resolving power of the method is to be realized. This means that the holographic plate must be uniform in optical thickness across its diameter to a fraction of a wavelength. Commercial plates suitable for electron diffraction patterns do not approach this perfection. Therefore, the electron diffraction patterns were photographically transferred to Kodak 131-02 holographic plates to form positive copies H_1, reduced 16-fold from the original negatives, H_e. This was accomplished by placing the negatives H_e in front of a uniformly illuminated area and photographing them. The fine-grained copies did not suffer a noticeable loss of detail; furthermore, across their greatly reduced aperture, they easily passed requirements for optical uniformity.

B. Optical reconstruction

Illustrated schematically in Fig. 2 is the second stage of the holographic microscope, the image synthesizer. Its source is a 3 mW He Ne laser of 1 mrad divergence, equipped with a spatial filter consisting of a lens of 36 mm f.l. and a 26 μm pinhole. The emergent beam is transmitted without further modification through lens 1 (f.l. =49 cm) and the hologram. At a distance 97 cm beyond the lens an image amplitude F_m is formed, superposed on a brilliant Airy pattern F_0—a pattern consisting of a central disk encircled by a great number of diffraction rings with radii determined by the aperture of the circular hologram. A considerable obscuration of the desired image by the Airy pattern is inevitable unless steps are taken to filter out the unwanted waves. The following practical way to do this was suggested by Professor Emmett Leith.[8] At the image plane is placed a small beam stop which screens through the third Airy ring, dropping the integrated Airy intensity by about 95%. Lens 2 (f.l. =43 cm), located 58 cm beyond the image, projects the reconstructed image (which begins somewhere between the seventh and tenth Airy rings) on to an ocular. Note that the molecular image is formed from the first-order interference fringes of light diffracted by the hologram whereas the Airy pattern is generated by light undiffracted by the hologram but scattered, instead, by the edge of the diaphragm surrounding the hologram. Therefore, at diaphragm D placed at the image of the hologram projected by lens 2, the surviving vestige of the unwanted Airy pattern shows up as a sharp, bright circle constituting the image of the holographic aperture. This can be largely skimmed off by diaphram D without removing much of the image of the hologram. Therefore, at a small cost of resolving power (the ratio of the radius of diaphragm D to the radius of the holographic image at D) most of the undesirable amplitude F_0 can be separated from the image amplitude, F_m. Unfortunately, the filter leaves a conspicuous artifact in the form of a bright ring outside the shadow of the beam stop.

Reconstructed images can be viewed or photographed through the ocular shown in Fig. 2. Images were recorded on Kodak Ektapan film 4162. Because it is not a trivial matter to determine the exact magnification of the image, as it arrives at the emulsion in the camera, solely from the geometry and effective focal lengths of the various lenses used, an alternative scheme was employed. A Ronchi grating with 100 lines/in. was substituted for hologram. Its rulings, acting as holographic fringes, produced easily measured spots on photographic plates taken with the camera in its normal position. From the spot separations, the magnification in the optical synthesizer could be calculated simply and precisely for given camera settings, compensating for film shrinkage during processing, as well. Unfortunately, experimental settings varied slightly from run to run, making the magnifications uncertain by about 5%, a fact which was uncovered only after circumstances required the termination of the experimental work.

III. EXPRESSIONS FOR THEORETICAL IMAGE INTENSITIES

A. Molecular diffraction patterns

It is convenient to express calculated intensities of diffraction patterns, both the original electron patterns and the optical Fraunhofer patterns derived from them, in terms of the natural scattering variable $s_i = (4\pi/\lambda_i) \times \sin(\theta_i/2)$. The radius, $b_i = L_i \tan\theta_i$, of the pattern is a convenient impact parameter to be used in the next stage of the calculation. In the following, the associated conversion from s to b will be understood, and we can express the intensity of electrons recorded at the photoplate as

$$I(b_e) = I_{at}[1 + M(s_e)], \tag{2}$$

where I_{at} is given by Eq. (1) and where $M(s_e)$ is the reduced molecular intensity

$$M(s_e) = 2\sum_{i<j}\sum A_{ij} \exp(-l_{ij}^2 s_e^2/2)(\sin s_e r_{ij})/s_e r_{ij} \tag{3}$$

if the interatomic radial distribution function of atom i relative to atom j is assumed to be Gaussian with a

mean-square amplitude of vibration l_{ij}^2. Coefficients A_{ij} in Eq. (3) are defined by Eq. (6) of Paper I.[1]

B. Reconstructed image intensities

As shown in Ref. 4, the Fraunhofer amplitude $F(b_2)$ received at the first image plane of Fig. 1 is

$$F(b_2) = \int \exp(\mathbf{s}_2 \cdot \mathbf{b}_1)\, U(b_1)\, d^2 b_1 \,, \tag{4}$$

where $U(b_1)$ is the amplitude of light transmitted through the hologram H_1; $\mathbf{b}_1$ is impact parameter $\mathbf{b}_e$ reduced by factor R when H_1 is copied from the original electron hologram H_e; and image radius b_2 is very nearly $(L_2\lambda_2/2\pi)s_2$. Because $U(b_1)$ is axially symmetric, Eq. (4) can be partly integrated to yield

$$F(b) = 2\pi \int_{s_{min}}^{s_{max}} J_0(sb)\, U(s)\, s\, ds \,, \tag{5}$$

where, for convenience, we express the image radius b in terms of its original molecular dimensions and convert the holographic impact parameter back to s, numerically equal to the original electron scattering variable s_e. It is understood that the actual image is enlarged by the magnification $RL_2\lambda_2/L_e\lambda_e$. Integration limits in Eq. (5) represent the range over which the filter Φ transmits electrons.

In Paper I it is found that

$$\begin{aligned} U(s) &= C\exp(KI_{at})\exp[KI_{at}M(s)] \\ &\simeq C\exp(KI_{at})\,[1 + KI_{at}M(s) + \cdots] \\ &\equiv U_0(s) + U_m(s) \end{aligned} \tag{6}$$

where C and K are experimental constants. Because transmitted amplitude $U(s)$ is a sum of two terms U_0 and U_m, the Fraunhofer amplitude $F(b)$ of Eq. (5) is a sum of the corresponding terms F_0 and F_m mentioned previously. It is worth noting that, when the standard Hurter and Driffield photo response law of emulsions[9] is followed in the holographic plate H_1, the constant K is given by $2.303\ \Gamma A_e/2I$ (note that A_e and I are proportional to each other). From this, the following important conclusion can be drawn. If the absorbance in the original electron pattern is adjusted to the value

$$A_e = 2/2.303\ \Gamma \tag{7}$$

or about 0.43 if Γ has a value of 2, an x-percent variation in the original absorbance A_e will be reproduced as an x-percent variation in transmitted amplitude $U(s)$ of Eq. (6). A larger A_e will exaggerate and a smaller A_e will wash out variations in U.

C. Optimum conditions

Let us consider the conditions leading to the most ideal image we can expect from this type of approach. It is apparent that the best images would be those for which (1) the incident electron wavelength is so small and sector filter so perfect that limits s_{min} and s_{max} in Eq. (5) can be taken as zero and (effectively) infinity, respectively, thereby yielding maximum resolving power; (2) the obscuring amplitude $U_0(s)$ of Eq. (6) is perfectly filtered out; (3) the sector-filter function Φ makes I_{at} a constant; (4) the incoherent subject scattering [i.e., the S_i of Eq. (1)] has been removed, say by a velocity analyzing filter, to make coefficients A_{ij} of Eq. (3) constant at very small s_e; and (5) $KI_{at}M(s)$ is small enough to make the molecular amplitude $U_m(s)$ accurately proportional to the reduced molecular intensity $M(s)$. If all five conditions are satisfied for calculated images, we shall refer to the images as "optimum." Effects of relaxing the requirements (1)–(5) individually or in combination are easily calculated by making the corresponding changes in Eqs. (5) and (6) before carrying out the computation of the image intensity $[F(b)]^2$.

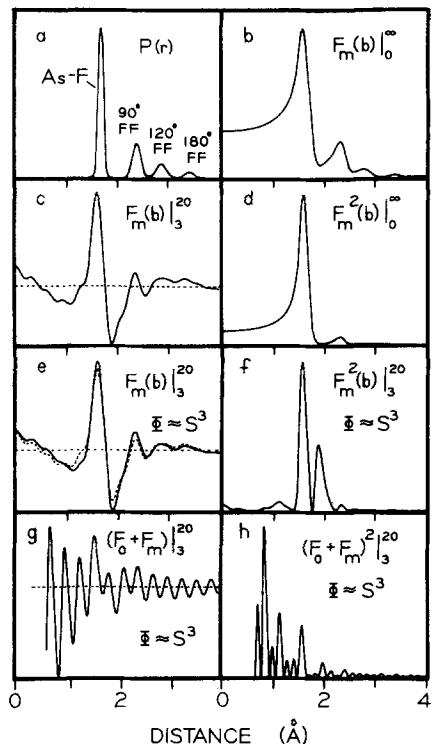

FIG. 3. Theoretical representations of molecular information for AsF_5 as calculated according to the parameters of Ref. 5 and assumed experimental conditions listed below. (a) Radial distribution function plotted against internuclear distance, r. (b) "Optimum" molecular image amplitude (see Sec. III. C of the text) as a function of molecular impact parameter b. (c) Molecular image amplitude reconstructed from hologram ideal between experimental limits $3 \le s \le 20$ but blocked off elsewhere. (d) Optimum molecular image intensity. (e) Molecular image amplitude reconstructed from hologram, $3 \le s \le 20$. Solid line, r^3 sector filter. Dashed line, optimum sector filter [same as curve (c)]. (f) Molecular image intensity corresponding to conditions of curve (e). Note: in curves (b)–(f) it is assumed that the undesirable amplitude F_0 has been completely filtered away. Curves g and h retain F_0 in full and illustrate how severely the Airy pattern obscures the molecular images in the absence of filtering. Curves go off scale inside $b = 0.6$ Å. (g) Unfiltered amplitude. (h) Unfiltered intensity. Vertical scale arbitrary in all curves. Filtered images use $s_e \le 0.9\, s_e^{max}$ because diaphragm D skims off the outer 10% of the image of the hologram.

IV. CALCULATED IMAGES

A. Case of one dominant scatterer

Since the images are axially symmetric, it is sufficient to plot them as a function of b, the image radius. Plotted in Fig. 3 are various representations of molecu-

lar information calculated for the molecule AsF_5, a trigonal bipyramid with five fluorine atoms ($Z=9$) nearly equidistant from the much heavier element arsenic ($Z=33$). In Fig. 3(a) is shown the radial distribution function $\sum_i \sum_j' Z_i Z_j P_{ij}(r)$ displaying the bonded As–F and various nonbonded F $\cdots$ F interatomic distances. Figures 3(b)–3(f) illustrate calculated image amplitudes $F(b)$ or image intensities $[F(b)]^2$ corresponding to a variety of reconstruction conditions. As expected from Eqs. (18)–(20) of Paper I,[1] it is the amplitude, not intensity, which bears the closest relation to $\rho^P(b)$, the rotationally averaged molecular density projected onto an image plane. Portraying an "optimum" image amplitude, Fig. 3(b) corresponds to a superposition of spherical shell images, one for each internuclear distance in the molecule, each one with an appearance resembling that sketched in Fig. 1 of Paper I. Corresponding more closely to an intuitive idea of what a rotationally averaged molecule should look like while spinning about its heavy atom is Fig. 3(d), the optimum image *intensity*. Subsidiary nonbonded peaks, which were prominent in the amplitude plotted in Fig. 3(b), are inconspicuous when the amplitude is squared. This is as it should be according to conventional holographic theory; in the language of holography, the subsidiary peaks correspond to the subordinate subject wave (fluorine waves) squared while the main peak is due to the cross term between the subject and reference waves. In holographic images the subject wave squared is a nuisance. In molecular images, where information is lost in the rotational averaging, the subject wave squared is a source of useful information.

Unfortunately, no rotating sector filter functions Φ have been achieved experimentally which are precise over the full range from $0<s<s_{max}$. Inevitably, there is a lower practical limit inside of which the transmission is blocked off. In our work s_{min} was about 3 Å^{-1}. This gives a dark central spot in the hologram H_1 which we have represented approximately in our calculations by setting the transmitted amplitude, $U(s)$ in Eq. (5), equal to zero inside s_{min}. As can be seen in Figs. 3(c)–3(h), this modest alteration of the s range has a large effect on the reconstructed patterns. As is well known to electron diffractionists, the range of data $0<s<s_{min}$ contributes little information about peak *positions*, if s_{min} is small, but it contributes almost the whole of the peak *areas*. Therefore, the deletion of $U(s)$ inside s_{min} introduces broad troughs under each peak of $F(b)$ to make the total area nearly zero. Even though the distortion is large, the peak positions in the image amplitudes, $F(b)$, remain easily recognizable. This is apparent in Figs. 3(c) and 3(e). Such a favorable state of affairs is lost in the image *intensity*, where the squaring of the amplitude converts the negative troughs to "false" peaks which may be much larger than some of the real peaks. These are evident in Fig. 3(f).

Requirement (3) of Sec. C, that the electron filter function Φ be adjusted to make I_{at} of Eq. (1) a constant for optimum reconstructions, is examined in Fig. 3(e). Here, it can be seen that a nonoptimum "r^3" sector does nearly as well as an optimum sector; at least it does if the image filter removes all of the unwanted amplitude U_0 of Eq. (16). Distortions due to the s_{min} cutoff are more serious.

In all of the reconstructions discussed above, calculations were based on a perfect subtraction of the unwanted amplitude U_0 transmitted through the hologram. For sake of comparison, Figs. 3(g) and 3(h) depict the results of retaining the full amplitude, U_0, transmitted through a hologram H_1 copied from a diffraction plate H_e recorded with a maximum absorbance of 0.6. The image is largely obscured by the Airy pattern. In principle, it is possible to filter out amplitude U_0 quantitatively, as discussed in Paper I. In practice, it is far simpler to adopt the alternative filter diagrammed in Fig. 1 and discussed in Sec. II B. A theoretical treatment of this filter is beyond the scope of this paper but has been outlined elsewhere.[10]

Condition (4) of Sec. C, the filtering out of the electronically inelastic scattering, would be extremely difficult and of little practical utility. If all other conditions were met, condition (4) would have to be met to yield undistorted images of $\rho^P(b_a)$. On the other hand, since the main deleterious effect of the inelastic scattering is to make the coefficients A_{ij} of Eq. (3) drop to zero at very small scattering angles, usually inside the value of s_{min} achieved in practice, the retention of inelastic scattering causes little additional harm if the sector filter is blocked off inside s_{min}, anyway.

Condition (5) of Sec. C is met sufficiently well, if absorbances in H_e are kept under 0.6 or so, that distortions caused by its breakdown are minor compared with the others shown in Fig. 3.

B. Case of an excessively heavy dominant scatterer

If the atom selected to scatter the "reference wave" has a very high atomic number, the incident electron wave is so highly distorted by the field of the atom that the hologram produced cannot reconstruct a faithful image when illuminated by an optical plane wave. The basis for this can be seen in the requirement that the coefficients A_{ij} of Eq. (6), Paper I, must be constant, in order to make the crucial integral, Eq. (14) of Paper I, valid. If Eq. (14) is valid and conditions in Sec. III C of the present paper are met, the reconstructed image amplitude is a true facsimile of the projected molecular density, $\rho^P(b)$. A severe failure of the Born approximation for atomic scattering will, however, lead to a large phase shift, $\eta_i(s)$, in the atomic scattering factor of heavy atom i and ultimately split the ijth peak in the Fourier transform of the intensity into two components if atom j is light.[11] For 40 kV electrons, this split becomes quite noticeable when the difference in atomic number exceeds 50. Illustrating the effect is Fig. 4, the image amplitude calculated for ReF_6 ($Z=75$ for Re, 9 for F) under conditions satisfying all requirements of Sec. III C for "undistorted" images.[12]

In principle, a simple phase modulation could be introduced into the reconstruction beam, via a weak lens, to compensate for the peak splitting of one image but not of its "twin." Or a rather drastic amplitude and phase modulation to compensate for a given $\cos(\eta_i - \eta_j)$

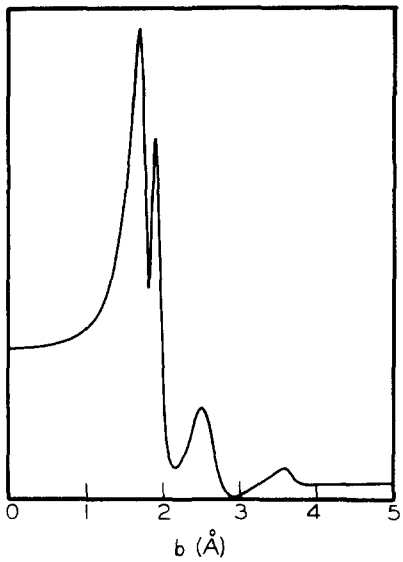

FIG. 4. Theoretical image amplitude for ReF_6 corresponding to $0 < s < \infty$. Note that the peak inside $b = 2$ Å is split even though it corresponds physically to a singly peaked Re–F distribution. Splitting is due to the strong phase shift $\eta(s)$ in the scattered wave from the heavy atom Re.

of Eq. (3) could remove the splitting of the ij peak if desired. The practical value of such a scheme is not immediately evident.

C. Case where no single atom dominates

Image intensities, $[F_m(b)]^2$, of molecules such as AsF_5 with a single heavy scatterer, exhibit only a single strong feature, the rotational average shell of light atoms [cf. Fig. 3(d)]. In an attempt to produce images distinctly showing more features, we selected two examples, SF_5Cl (hexacoordinated sulfur) and CF_3OOCF_3, both of which have radial distribution functions [see Figs. 5(a) and 5(b)] showing several strong peaks as well as lesser ones.[6,7] The former example has two moderately strong comparable scatterers, Cl and S. All atoms are comparable in the latter. Neither, then, satisfies the conventional holographic requirement for a single strong reference beam. Each can be regarded as generating several reference beams as well as "subject waves." Theoretical "images" for the two molecules are presented in Figs. 5(c)–5(h). These images are markedly more complex than the corresponding images 3(b)–3(d) for AsF_5. Image intensities $[F_m(b)]^2$ display several prominent spurious features arising from the cutoff of holographic transmission inside $s_{min} \approx 3$. These false peaks are identified by arrows for later comparison with experiment.

V. EXPERIMENTAL IMAGES

A. Effect of optical filter

Before discussing the molecular information visible in the optical reconstructions it is necessary to show how the reconstructions are influenced by the optical filter diagrammed in Fig. 2. If no filter is used, that is, if the stop and aperture in Fig. 2 are removed, the image is badly obscured, as shown in the photograph of AsF_5 reproduced in Fig. 6(a). This photograph may be compared with the corresponding calculated image of Fig. 3(h), which agrees with it almost perfectly through the 20th Airy ring. Inserting the stop without the diaphragm removes most of the central Airy disc and the innermost rings, but it scarcely influences the Airy rings obscuring the molecule. Inserting the diaphragm but not the stop merely expands the Airy pattern radius slightly without reducing the Airy intensity relative to that of the desired image. As shown in Fig. 6(b), however, the combination of stop and diaphragm greatly reduces the unwanted pattern relative to that of the molecular image. Unfortunately, the filter does produce a prominent artifact which might confuse an observer unfamiliar with the filter. This is mainly in the form of a bright ring of radiation, scattered by the stop and not completely skimmed off by the diaphragm, which appears outside the image of the stop but inside the molecular image. Its appearance is shown in Fig. 6(c), a photograph taken under the same conditions as those of 6(b) except that the hologram H_1 was removed.

B. Filtered molecular images

Pictures of AsF_5, SF_5Cl, and CF_3OOCF_3, respectively, are shown in Figs. 7(a)–(c). Let us disregard the artifacts corresponding to Fig. 6(c) which are conspicuous in all images. Arsenic pentafluoride shows up as

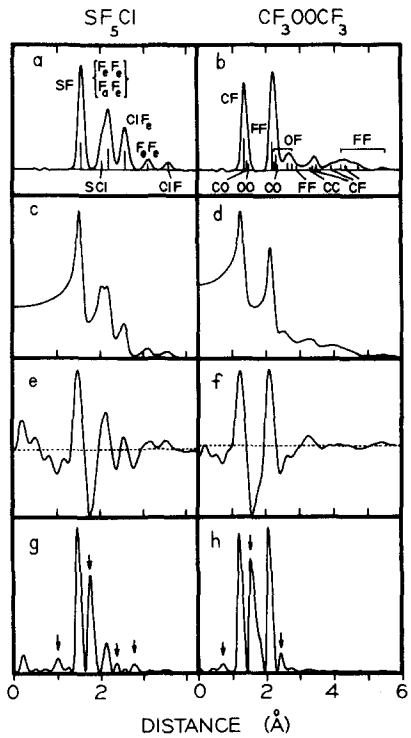

FIG. 5. Experimental radial distribution functions [(a) and (b)] and theoretical projected images [(c)–(h)]. Curves (a), (c), (e), and (g) pertain to SF_5Cl, while (b), (d), (f), and (h) apply to CF_3OOCF_3. Curves (c) and (d), optimum image amplitudes. Curves (e) and (f), image amplitudes corresponding to $3 \leq s \leq 20$ and an r^3 sector filter. Curves (g) and (h), image intensities corresponding to the conditions of (e) and (f). Perfect image filtering assumed in (c)–(h). False peaks in (b) and (h) are indicated by arrows.

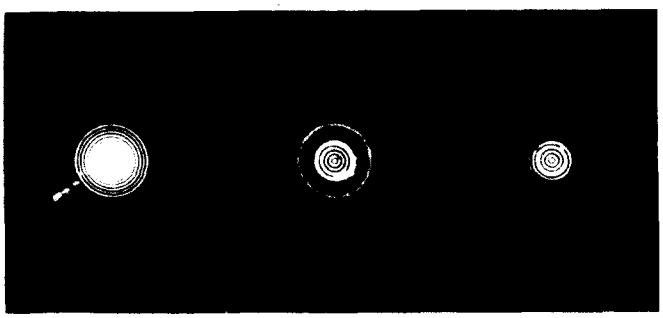

FIG. 6. Effect of optical filter diagrammed in Fig. 2. (a) Unfiltered image of AsF_5 partly obscured by Airy diffraction rings. rings. (b) Filtered image of AsF_5 exhibiting spurious rings at 0.9 Å and inwards due to filter. (c) Intensity produced by filter without a hologram present. Since $U_0(s)$ is nonuniform in (b) due to the nonoptimum sector function Φ but is uniform in (c), the ratio of the spurious ring intensities at 0.6 Å and 0.9 Å is reversed between photographs (b) and (c).

the projection of its spherical shell of fluorines surrounded by a weak "false" peak and a vestige of the 2.3 Å F ··· F distance. The more complex molecules display a richer spectrum of peaks, as anticipated. Ring radii at peak maxima of the image plates could be measured to a few thousandths of a centimeter with the aid of digital microdensitometer readings made every 0.005 cm on the images as they were spun to average out grains in the emulsions. Results for SF_5Cl and CF_3OOCF_3, converted to angstrom units, are listed in Tables I and II, where interatomic experimental distances are compared with those found from theoretical curves. The latter are calculated in the manner of the curves in Figs. 5(g) and 5(h) to take into account the foreshortening in the projected density and the finite electron wavelength and numerical aperture. Agreement between observed and calculated peak positions is reasonably satisfactory, particularly in view of the fact that no corrections were made for the perturbations introduced by the remnants of the Airy pattern surviving the filtering. From the substantial shift inwards of the internuclear peak positions from mean r_g values to the maxima in $\rho^P(b)$, it is clear that careful foreshortening corrections would be essential if the present method were to be used to measure internuclear distances.

TABLE I. Positions (in Å) of peak maxima in SF_5Cl reconstructions.

Peak	r_g[a] obs	b(max)[b] Calc	b(max)[c] Recon #20	b(max)[c] Recon #21
S–F	1.569	1.486	1.476	1.475
False	···	1.776	1.783	1.783
SCl, FF (mean)	2.194	2.105	2.086	2.082
False	···	2.374	2.386	2.394
ClF	2.597	2.575	···	···

[a]Reference 6.
[b]From theoretical image intensity based on Eq. (5) and structure of Ref. 6.
[c]Owing to scale factor errors due to unreproducible camera placement (see text) distances have been arbitrarily multiplied by the factor 1.031.

TABLE II. Positions (in Å) of peak maxima in CF_3OOCF_3 reconstructions.

Peak	r_g[a] Obs	b(max)[b] Calc	b(max)[c] Recon #17	b(max)[c] Recon #15
CF, CO, OO (mean)	1.349	1.261	1.272	1.265
False	···	1.577	1.572	1.570
FF, CO···	2.199	2.120	2.102	2.105
False	···	2.416	2.402	2.407
OF, FF[d]···	2.617	2.627	2.642	2.645
False		2.750	2.767	···
CF, OF···	3.313	3.271	3.280	···

[a]Reference 7.
[b]From theoretical image intensity based on Eq. (5) and structure of Ref. 7.
[c]Owing to scale factor errors due to unreproducible camera placement, distances have been arbitrarily multiplied by the factor 1.042.
[d]Due to effect of trough it occurs in, the peak in F_m appears as a minimum in F_m^2.

VI. DISCUSSION

In Paper I it was proposed that molecular images (rotationally averaged) can be reconstructed optically by using suitably recorded electron diffraction patterns as holograms. This possibility has been fully realized in the present study. We have also observed the extra molecular information theoretically present in the more complex "images" obtained when conventional holographic requirements—for only a single "reference wave"—are overridden. It is worthwhile to put the present research into perspective and discuss its relationship to other diffraction techniques and microscopy.

From the viewpoint of physical optics, diffraction, holography, and microscopy share a common basis. In the first stage of each procedure, a sample (subject) is irradiated and the scattered radiation intercepted by a diffraction plate, hologram, or objective lens, carries a signal that is the Fourier transform of the scattering density in the subject. A digital analysis, optical interference, or lens focusing procedure is then adopted to convert that signal into an interpretable form. The reliability of information about the subject so derived depends crucially upon the technical limitations in each

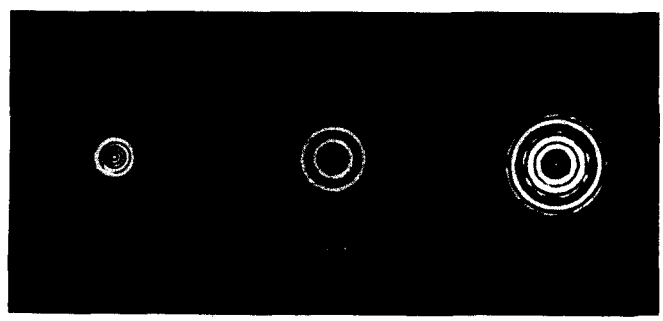

FIG. 7. Photographs of (a) AsF_5, (b) SF_5Cl, and (c) CF_3OOCF_3. Note that the "false peaks" are appreciably weaker in the photographs than in the calculated curves [Figs. 3(f), 5(g), and 5(b)]. This is because the actual holograms were not infinitely black in the region $o < s < s_{min}$ as implied in the idealized expression of Eq. (5) by taking $U(s) = o$ in this range. The real peaks are in good agreement with the calculated peaks. Scale bar 1 Å.

type of experiment. In principle, if a perfect reference beam of large numerical aperture could be coherently superposed, at will, upon a diffraction pattern to allow phase information to be retained in a diffraction plate, or if it were possible to graft holograms taken over various ranges of scattering variable s onto each other, or if it were possible to use an aberration-free lens of large numerical aperture, the three different techniques would, in principle, yield comparable resolving powers and accuracies. In practice there is a problem of phase loss in diffraction, of limited angular range of "sector filter" in the present variant of holography (as well as phase loss), and of small numerical aperture in electron microscopy. Moreover, the first two methods, in their gas-phase form, suffer from losses due to orientational averaging.

Let us first consider resolving power. Note that, in Table II, a distance of 0.5 Å in CF_3OOCF_3 is well resolved in our optical reconstructions. Under the present experimental conditions, the ultimate resolution limit should be about 0.15 Å. A resolution limit of perhaps 1/3 of this is possible in gas diffraction patterns recorded out to currently attained numerical apertures—though a resolution this fine or finer would be difficult to verify experimentally since amplitudes of vibration tend to be 0.05 Å or larger. The present resolution is an order of magnitude finer than that attained in the best conventional micrographs, however, because of the spherical aberration which limits the useful aperture of objective lenses. Of course, the microscope is much more versatile in the types of subjects it can study.

The ultimate precision attainable in the present technique is not yet firmly established. Microdensitometer traces show that the ratios of peak positions between different plates of the same molecules are constant to within about two parts per thousand, suggesting that an accuracy of this quality would be possible if steps were taken to ensure an optimum projector lens setting and a reproducible camera position. In our current, trial configuration, these settings are made quite crudely with the result that our scale factor is unstable by several percent, as pointed out in the footnotes of Table II. On the other hand, an examination of Fig. 5, which compares experimental electron diffraction radial distributions with theoretical holographic reconstructions, indicates the advantage of decoding electron diffraction plates by numerical analysis instead of by optical reconstruction. Fourier sine transforms of corrected, composite data over a large range of scattering variable are superior to Bessel function transforms of raw data over the range of one sector filter. Therefore, the optical reconstruction method is unlikely to be competitive, in the case of gas molecules, with the more conventional methods. However, if it had appeared many years ago, before the availability of fast digital computers, the optical method might have been of some practical use in structure analysis.

At its present stage of development the holographic method is more of a curiosity than a finished research tool. It serves to remind us that we have had within our capability, for many years, the possibility of seeing and photographing quite directly the images of gas phase molecules—of measuring interatomic distances with a ruler—by optical reconstruction from standard diffraction plates. It suggests ways, simple conceptually but terribly difficult in practice, of obtaining holographic views of oriented molecules, possibly adsorbed on surfaces. Perhaps, one day, by extensions of this technique, Gabor's vision of freeing electron microscopy from the tyranny of the spherical aberration of objective lenses will be fully realized.

ACKNOWLEDGMENT

This research was supported by a grant from the National Science Foundation.

[1]L. S. Bartell, J. Chem. Phys. **70**, 3952 (1979), preceding paper.
[2]D. Gabor, Nature (London) **161**, 777 (1948); Proc. R. Soc. London Ser. A **197**, 454 (1949).
[3]L. S. Bartell, in *Techniques of Chemistry: Physical Methods in Chemistry*, edited by A. Weissberger and B. W. Rossiter (Interscience, New York, 1972), 4th ed., Vol. 1, Part 3D, pp. 125–158.
[4]L. S. Bartell, Optik **43**, 403 (1975).
[5]F. B. Clippard and L. S. Bartell, Inorg. Chem. **9**, 804 (1970).
[6]C. J. Marsden and L. S. Bartell, Inorg. Chem. **15**, 3004 (1976).
[7]C. J. Marsden, L. S. Bartell, and F. P. Diodati, J. Mol. Struct. **39**, 253 (1977).
[8]E. N. Leith, Photogr. Sci. Eng. **6**, 75 (1962).
[9]See R. J. Collier, C. B. Burkhardt, and L. H. Lin, *Optical Holography* (Academic, New York, 1971), Chap. 2.
[10]L. S. Bartell (to be published).
[11]R. Glauber and V. Schomaker, Phys. Rev. **89**, 667 (1953).
[12]For an experimental study of ReF_6 revealing the Re–F peak splitting, see E. J. Jacob and L. S. Bartell, J. Chem. Phys. **53**, 223 (1970).